J Bionic Eng 15 (2018) ???–???
DOI: https://doi.org/12345-018-1234-x

Journal of Bionic Engineering
http://www.springer.com/journal/42235

Hybrid laser ablation and chemical modification for fast fabrication of bio-inspired super-hydrophobic surface with excellent self-cleaning, stability and corrosion resistance

Zhen Yang[1, 2], Xianping Liu[1], Yanling Tian[1, 2, *]

1. *School of Engineering, University of Warwick, Coventry CV4 7AL, UK*
2. *Key Laboratory of Mechanism Theory and Equipment Design, Ministry of Education, Tianjin 300350, China*

Abstract

Although laser ablation is considered as a facile technique to fabricate bio-inspired super-hydrophobic surfaces, the issue is that the initial laser treated metallic surfaces show super-hydrophilic property. It will take a long period to reach super-hydrophobic state under ambient air. It is reported that these super-hydrophobic surfaces could be easily damaged by thermal heating effect or interaction with other liquids, causing uncontrolled loss of super-hydrophobicity. In this study, a stable super-hydrophobic aluminum surface was rapidly fabricated via the hybrid laser ablation and surface chemical modification of (heptadecafluoro-1, 1, 2, 2-tetradecyl) triethoxysilane (AC-FAS). Surface morphology and chemistry were systematically investigated to explore the generation mechanism of super-hydrophobicity. The water contact angle of the treated surfaces can reach up to 160.6 ± 1.5º with rolling angle of 3.0 ± 1.0º, exhibiting perfect self-cleaning capability, long-term stability, and excellent chemical stability in acidic as well as alkaline solutions. The potentiodynamic polarization tests implied that the super-hydrophobic surfaces showed better anti-corrosion performance. This hybrid laser ablation and surface chemical modification is very time-saving and low-cost, which offers a rapid way for quantity production of super-hydrophobic surface on aluminum material.

Keywords: bioinspiration, nanosecond laser, super-hydrophobic, chemical stability, corrosion resistance, self-cleaning, long-term stability

1 Introduction

Surface wettability plays a significant role in various physical, chemical and biological processes [1]. Some natural plants and animals have developed particular functional surfaces to respond extreme challenges: lotus leaves with self-cleaning character to maintain themselves clean in dirty environment [2], desert beetle harvesting water vapor to survive in dried environment [3] and the water strider walking on the water due to its legs facilitating floatation [4], to name a few. Inspired by nature, super-hydrophobic surfaces, generally defined when a water contact angle (WCA) greater than 150°

***Corresponding author:** Yanling Tian
E-mail: Y.Tian.1@warwick.ac.uk

and rolling angle (RA) less than 10°, have attracted extensive attention owing to their great significance in academic research and potential in practice [5-6]. These super-hydrophobic surfaces play a significant role in various practical applications, such as self-cleaning, corrosion inhibition, anti-bacteria, oil/water separation and drag reduction [7-12]. Many super-hydrophobic surfaces can be observed in nature and it is well accepted that the super-hydrophobicity is governed by the combination of hierarchical micro/nano structures and surface chemistry [13-14]. It is reported that the bio-inspired super-hydrophobic surfaces have been successfully fabricated on many materials including metals, polymers and ceramics by different manufacturing methods, such as nanoimprinting, casting, chemical etching, electrodeposition, laser ablation and so on [15-20].

Among above mentioned materials, it is well considered that metallic surfaces are widely utilized in various applications, for example, heating/cooling pipes, ship-buildings and outdoor structures [21]. Laser ablation has been regarded as one of the facile methods and thus widely used to create man-made metallic super-hydrophobic surfaces. But, immediately after laser process, the initial laser-induced surfaces show a hydrophilic nature rather than hydrophobic, and it will need a long period, from couple of days to months, to reach stable super-hydrophobic property in the ambient air. According to previous studies, nanosecond laser ablated copper/brass surfaces may need 11 or 12 days to reach super-hydrophobic state [22]. In some cases, laser ablated stainless steel and aluminum surfaces required more time, around 30 days to achieve super-hydrophobicity [23-25]. In our previous work, we also investigated the nanosecond laser induced wettability transition on Inconel 718 and titanium surfaces, and the results indicated that the two materials would need 20 days and 28 days to achieve super-hydrophobicity, respectively [26-27]. This phenomenon is a severe barrier in industry for quantity production of super-hydrophobic surfaces because of the long process time and limitation of economic efficiency.

Furthermore, previous research reported that the gradual contact angle conversion from

super-hydrophilicity to super-hydrophobicity was ascribed to the spontaneous chemisorption of airborne contaminations onto the laser-induced rough surfaces [28-29]. This route of hydrophobization seems environmental-friendly and naturally reproducible. However, the durability and chemical stability of the chemisorbed airborne contaminations are very sensitive to the content, compositions and chemical structure of contaminations in ambient air. It is obvious that, without further treatment of the laser-induced surface, the physically adsorbed organic layer cannot be well ordered. Owing to the thermal heating or interaction with other liquid medium, such super-hydrophobic coating can be easily damaged, causing the uncontrolled loss of the super-hydrophobic behavior. As a result, this super-hydrophobic surface is not suitable for industrial, especially for outdoor, applications [30]. Thus, it is required to rapidly develop chemically stable and durable super-hydrophobic surfaces for practical applications in engineering.

In this work, a further process of surface chemical modification was introduced on nanosecond laser ablated surfaces to control surface chemisorption and reduce the wettability conversion period. The as-prepared surfaces showed a rapid super-hydrophobic property because of the presence of AC-FAS molecules. The processing time was significantly reduced to several hours. In order to systematically explore the formation mechanism of the as-prepared surface, the surface properties were comprehensively examined by contact angle instrument, scanning electron microscopy (SEM), stylus profilers, white light confocal microscopy, energy-dispersive spectroscopy (EDS) and X-ray photoelectron spectroscopy (XPS). The as-prepared super-hydrophobic surfaces showed outstanding chemical stability in various pH values, excellent self-cleaning capability and long-term stability in ambient air due to the controlled surface chemical compositions. In addition, the anti-corrosion performance of the received super-hydrophobic surface was also evaluated by potentiodynamic polarization tests in 3.5 wt. % NaCl solution. This study is expected to rapidly produce super-hydrophobic surfaces within a relatively short time for industrial application, and this approach

has promising prospect to other materials.

2 Materials and experimental methods

2.1 Materials

In this study, the 1060 aluminum material (high-purity 99.6%) was investigated. Commercial 1 mm thick sheet of aluminum was cut into square samples (20 mm × 20 mm) for experiments. AC-FAS [CF_3-$(CF_2)_7$-$(CH_2)_2$-Si-$(OC_2H_5)_3$] was purchased from Alfa Aesar Company. Absolute ethanol, acetone, sodium chloride, hydrochloric acid and sodium hydroxide were purchased from Beijing Chemical Works and used as received without further purification. Distilled water applied in the prepared solution and contact angle measurements was supplied by a commercial water purification system.

2.2 Preparation of samples and AC-FAS/ethanol solution

Before laser treatment, all the aluminum substrates were polished and washed by acetone, ethanol and deionized water in sequence in an ultrasonic bath each for 5 minutes to reduce the variation of laser beam absorption by contaminants. Then the rinsed substrates were dried under the compressed nitrogen. The AC-FAS/ethanol solution was prepared by mixing AC-FAS and ethanol and then reacting with water at room temperature. 0.25 g AC-FAS and 9.6 mL distilled water were subsequently added to 31.4 mL absolute ethanol under stirring for 10 min until a uniform AC-FAS/ethanol solution was obtained.

2.3 Nanosecond laser texturing

As shown in Fig. 1, a nanosecond Ytterbium pulsed fiber laser system (IPG photonics from Germany) was utilized in this work, which provided a laser beam with a wavelength of 1064 nm, output power of 10 W, pulse duration of 50 ns, repetition rate of 20 kHz. The focused laser beam with a spot diameter of 50 μm was delivered by a scanning head. Fixed on the working platform, the prepared aluminum substrates were irradiated by the moving laser beam with a constant scanning speed of 500 mm/s. The laser scanning strategy is illustrated by the dashed lines in Fig. 1. According to laser beam path, the laser ablated surfaces exhibited grid-patterned structure that could endow super-hydrophobic

surfaces with isotropic property [31]. The pitch was defined as the distance between adjacent laser beams. In this study, the pitch equaled in both directions, and the values of 40, 60, 80, 100 and 150 μm were selected. All the laser ablation experiments were carried out under the atmospheric conditions.

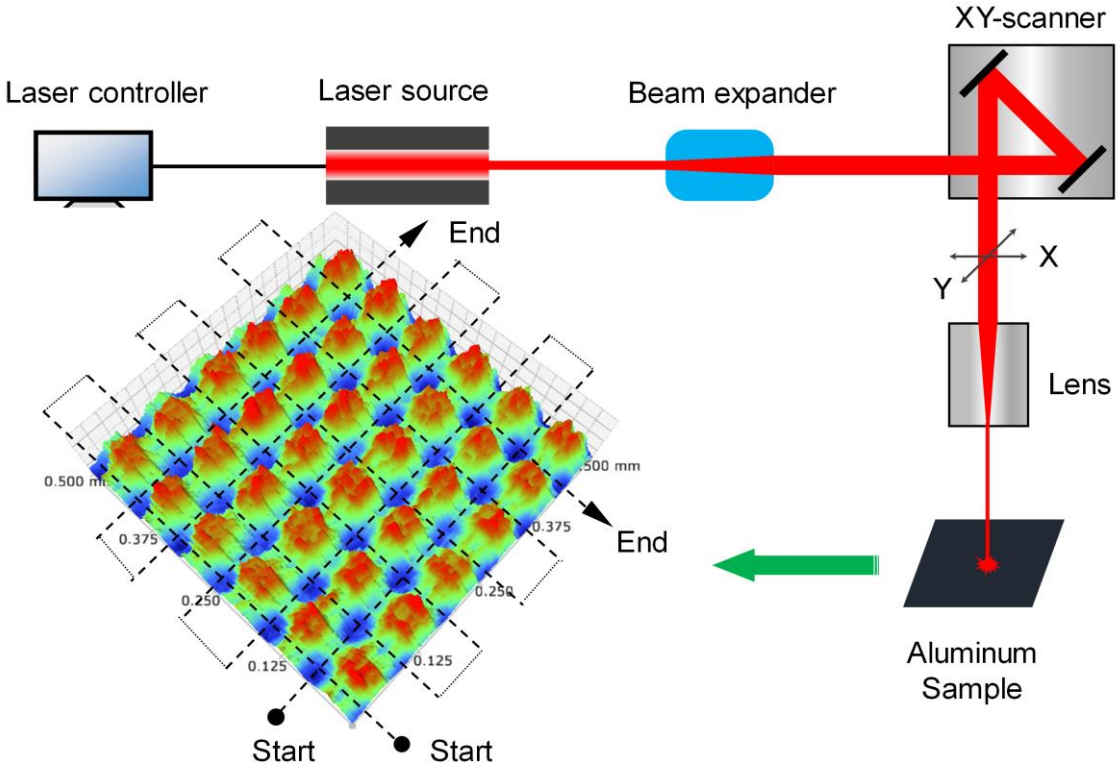

Fig. 1 Schematic of integrated laser system and the laser scanning strategy.

2.4 Surface chemical modification

The laser ablated surfaces were ultrasonically washed in deionized water for 5 minutes to remove the residual debris, followed by blowing compressed nitrogen to dry their surfaces. Subsequently, they were immersed into AC-FAS/ethanol solution for 2h to lower surface free energy under cleanroom condition. Finally, all the processed samples were flushed by deionized water and then dried at 60 ºC in oven for 30 minutes. The fabricated surfaces with different pitch were abridged as Al-40, Al-60, Al-80, Al-100 and Al-150, respectively. The pristine aluminum substrate was abridged as Al-I. Another pristine surface without laser ablation was also modified with AC-FAS/ethanol solution using the same method, which was abridged as Al-II for reference.

2.5 Characterization

The hydrophobicity of the samples was detected by measuring static WCA and RA using sessile drop technique (AST, VCA optima). An 8 μL distilled water droplet was dispensed on the samples at cleanroom conditions (constant temperature 25ºC, air humidity around 50%). For data reliability and result reproducibility, every sample was measured five spots to determine the contact angle value. Surface morphology characterization was performed by SEM (FEI, Quanta 250 FEG). Besides, stylus profilers (Bruker, Dektak) and white light confocal microscope (Zeiss, CSM700) were utilized to obtain 3D profile and surface roughness of the fabricated samples. EDS (Oxford instruments, X-Max 80) and XPS (Thermo Fisher Scientific, Escalab 250Xi) were utilized to analyze surface chemistry. The bouncing experiments were recorded using a high-speed video camera (NAC, HX-3E) with the sample frequency of 6000 frames per second.

Electrochemical corrosion resistance of the as-prepared super-hydrophobic surfaces was examined by potentiodynamic polarization test in a standard three-electrode cell configuration. A platinum electrode and a saturated calomel electrode (SCE) were utilized as the counter electrode and reference electrode, respectively. The pristine Al-I surface and fabricated super-hydrophobic Al-80 surface were used as the working electrode with a surface area of 1 cm^2 exposed to corrosion medium. The measurements were performed in 3.5 wt. % NaCl solution at room temperature by an electrochemical workstation (CHI660D, China). Before the electrochemical tests, the samples were immersed in corrosion solution for 15 minutes to make the electrochemical system stabilize. The potentiodynamic anodic polarization curves were obtained at a sweep rate of 10 mV/s. The corrosion current density (I_{corr}), corrosion potential (E_{corr}) were determined by Tafel extrapolation from the polarization curves.

3 Results and discussion

3.1 Wettability

The static WCA and RA were measured by using the 8 μL water droplet to investigate wettability of

the fabricated surfaces. Fig. 2a shows that the pristine Al-I surface was hydrophilic with a WCA of 85.0 ± 3.0º. After silanization process, the WCA of Al-II surface exhibited slight hydrophobicity although the low energy material of AC-FAS was utilized during the surface modification process. It is revealed that due to the absence of laser-induced micro/nano structures, the surface chemical modification is not the only factor to determine surface super-hydrophobicity. Noticeably, the WCAs beyond 150º were obtained for all the laser treated sample surfaces with the presence of AC-FAS, implying that the super-hydrophobic surfaces can be obtained by hybrid method of laser ablation and further surface chemical modification. It is also noted that due to the pitch effect, there was a significant increase for WCA from pitch value of 40 μm to 80 μm. With the further increase of pitch value, the WCA experienced a slight decrease. Thus, the Al-80 sample showed the largest contact angle around 160º, as shown in Figs. 2a and 2b. Fig. 2c shows that the Al-80 super-hydrophobic surface had an advancing contact angle (θ_A) of 161.3 ± 1.0º and a receding contact angle (θ_R) of 157.3 ± 1.0º, indicating that the Al-80 surface had very low contact angle hysteresis. Fig. 2d confirms that the water droplet can immediately roll off from the nearly horizontal super-hydrophobic surface without any adhesion (**Video 1**), which is in complete agreement with the advancing and receding contact angle shown in Fig. 2c. These results demonstrate that the super-hydrophobic surface had an ultralow RA around 3º, and thus this surface showed excellent self-cleaning property.

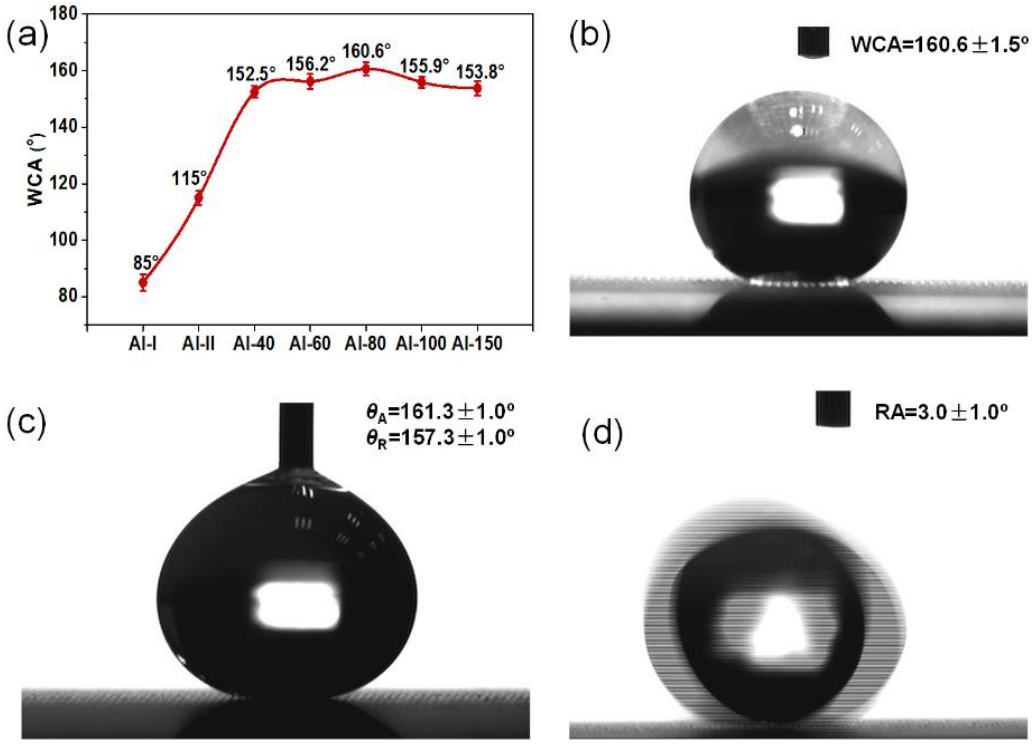

Fig. 2 (a) WCAs values on different aluminum surfaces, (b) WCA measurement of the Al-80 surface, (c) Advancing and receding contact angle measurement on the Al-80 surface, (d) Water droplet rolling off the Al-80 surface.

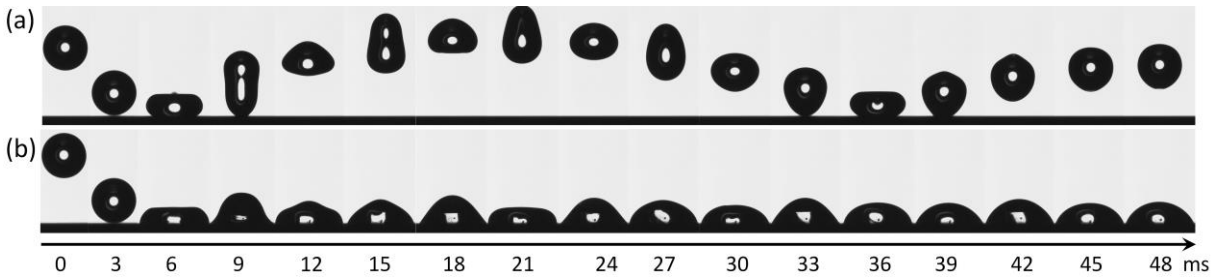

Fig. 3 Snapshots of distilled water droplet with 1.6 mm radius hitting on the (a) super-hydrophobic Al-80 surface, (b) bare Al-I surface.

To further investigate the performance of the fabricated super-hydrophobic surface, the bouncing experiments were carried out using a high-speed camera. Fig. 3a and 3b exhibit a series of photos of a droplet impacting the super-hydrophobic Al-80 surface and the bare Al-I surface, respectively. When the water droplet freely released from the needle, it firstly hit the target surfaces, and gradually deform at most because of the gravity and impact force. Then the impacting kinetic energy will convert into elastic potential energy. It is obvious from Fig. 3a that the water droplet can fully rebound off the super-hydrophobic surface due to the complete energy transformation. Besides, no residual droplet can

be noticed during the whole shock (**Video 2**), implying that the adhesive force between the droplet and the as-prepared surface was extremely low and could be ignored [32]. On the contrary, the water droplet will firmly stick on the bare aluminum surface and cannot rebound off the surface due to the high adhesive force, as shown in Fig. 3b. Then the water droplet will quickly reach a stable state after several up and down shocks (**Video 3**). The bouncing experiments clearly indicate that compared to the flat aluminum surface, the as-prepared surface showed excellent super-hydrophobicity with very ultralow adhesion. The water droplet can rebound off the super-hydrophobic surface and leave the surface without any without any residual liquid.

3.2 Surface morphology

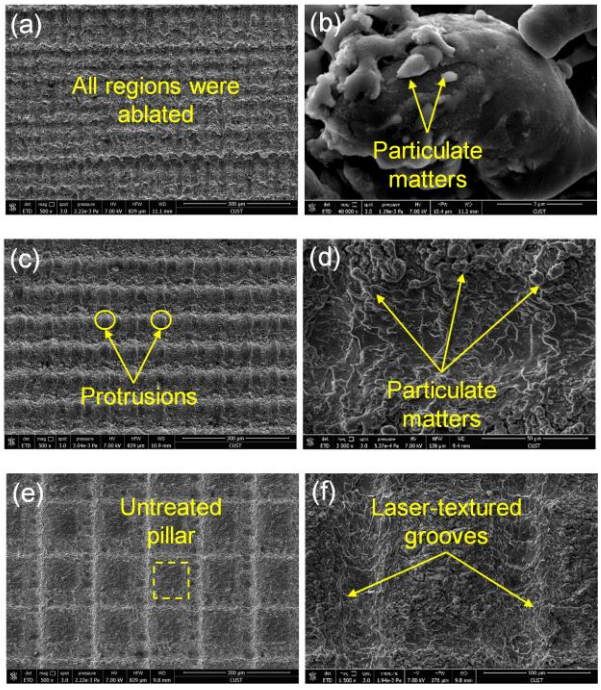

Fig. 4 SEM images of the laser-induced surface structures: (a, b) Al-40, (c, d) Al-80, and (e, f) Al-150.

Fig. 4 shows the SEM images of super-hydrophobic surfaces with different pitch. In this paper, in order to observe the distinct difference of the laser ablated samples, we only display the SEM images of Al-40 (Figs. 4a-4b), Al-80 (Figs. 4c-4d) and the Al-150 (Figs. 4e-4f). It is clearly noted that during the laser scanning process, the focused laser spot will travel along the designed path and the sample

surfaces were intensively heated and melted along the laser path, which created a localized melt pool. Subsequently, the melted materials would be removed from the laser path, creating the grooves. Due to the effect of rapid cooling and solidification of splashing material, it can be seen that the brim of the grooves was covered by the debris (i.e. the redeposited materials). However, when the pitch (40 μm) was smaller than the diameter of laser beam (50 μm), the small overlap of successive laser paths occurs. As a result, the whole surface will be modified by the melted materials (as shown in Fig. 4a). Thus, the ablated structure on this surface was much more uniform and different from the normal grid-patterned structures (as show in Fig. 4e). Interestingly, it can be observed from the high-magnified image that there were large number of particulate matters on the uniform surface, which can facilitate the fabricated surface to be more hydrophobic. As shown in Fig. 4b, many protrusions with the average diameter of 20 μm were created on Al-80 sample after laser texturing process and there also exist small nanoscale particles on these protrusions. Therefore, the special hierarchical rough surface texture can generate large space in which the air could be trapped, resulting in the suspension of liquid droplet on the fabricated sample. The high WCA can be described by the Cassie-Baxter equation [32-34]:

$$\cos\theta_{CB} = f_1 \cos\theta_0 - f_2 \qquad (1)$$

where f_1 and f_2 denote the fractional area of solid surface that is wetted and air in contact with liquid droplet; θ_0 (85º) and θ_{CB} (160.6º) denote the WCAs of the pristine Al-I surface and super-hydrophobic Al-80 surface, respectively. Given that $f_1 + f_2 = 1$, f_1 can be calculated at 0.052, inferring that the contact area between the droplet and the trapped air can reach up to 94.8% (the bright section clearly shown in Fig. 2b). Due to the absolutely hydrophobic air, the hierarchical structures with huge amount of trapped air can promote surface hydrophobicity. However, it can be clearly seen from Figs. 4e and 4f that the obvious untreated pillars dominate the fabricated surface when the pitch increases to 150 μm, leading to the decrease of WCA. This phenomenon may be ascribed to the increase of solid contact area for the water droplet as well as the decrease of surface roughness.

Table 1 Surface roughness of the investigated samples

Sample	Al-I	Al-II	Al-40	Al-60	Al-80	Al-100	Al-150
R_a (μm)	0.8 ± 0.1	0.8 ± 0.1	11.6 ± 1.0	14.5 ± 1.2	16.4 ± 1.5	14.2 ± 1.0	12.8 ± 0.9

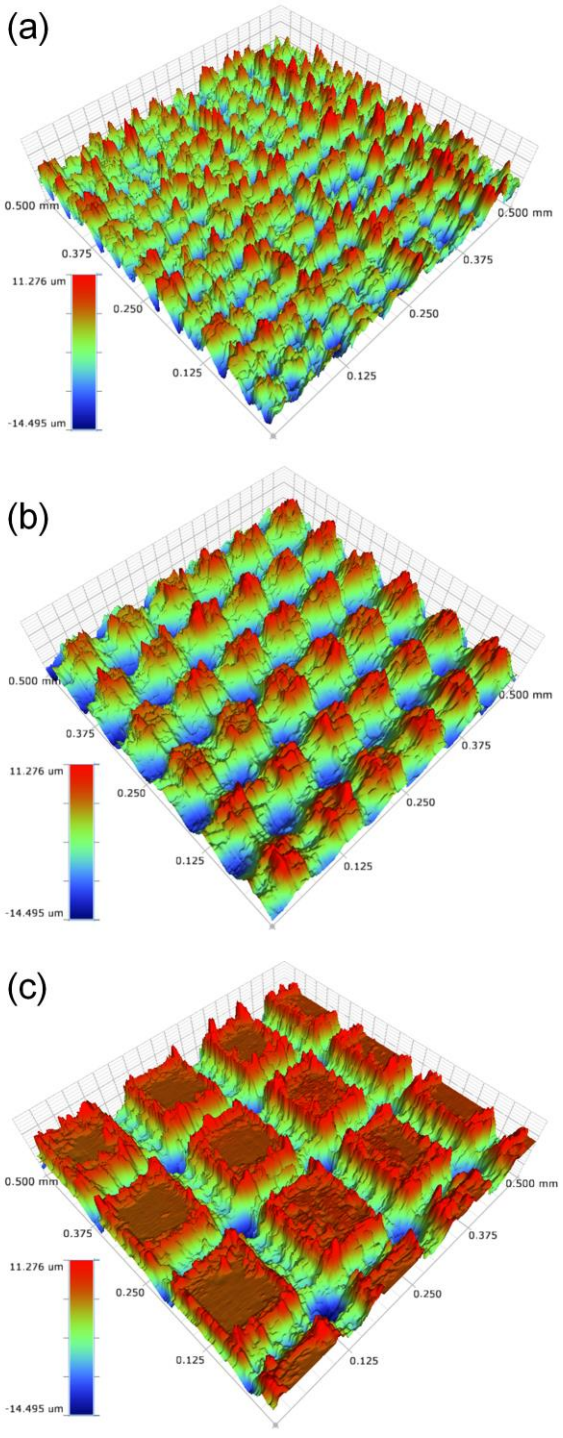

Fig. 5 3D profiles of the fabricated surfaces: (a) Al-40, (b) Al-80, (c) Al-150.

To investigate the relationship between surface roughness (R_a) and surface wetting property, 3D

profile and surface roughness of the samples were measured and displayed in Fig. 5 and Table 1. The 3D profiles of the sample surfaces are well in agreement with the SEM images that the Al-40 surface (Fig. 5a) showed a uniform structure after laser ablation. It is clear from Fig. 5b that the Al-80 sample was modified with many protrusions array that made the surface much rougher. However, the obvious grid-pattern was generated on the Al-150 surface, as shown in Fig. 5c). From Table 1, the pristine Al-I surface had a surface roughness value of about 0.8 μm. After heated in the oven with the presence of AC-FAS, there was no obvious change in terms of its surface roughness between Al-I and Al-II surfaces. However, the surface roughness increased from 0.8 μm to beyond 10 μm for the laser treated surfaces. Due to the pitch effect, the surface roughness showed a significant increase from the pitch value of 40 μm to 80 μm. However, the surface roughness of the laser ablated surface started to decrease for the further increase of pitch value. This is due to the growing proportion of untreated area, which agrees with the surface morphology shown in Figs. 4 and 5. As expected, the super-hydrophobic sample (Al-80) had the largest surface roughness of 16.4 ± 1.5 μm because its surface showed hierarchical structures with many nanoscale particles covered on micron size protrusions. The results confirm that the surface roughness had a close relationship with the surface wettability: the bigger surface roughness leads to larger WCA. It is reported that the rough surface with micro/nano structures is necessary for obtaining super-hydrophobic surfaces [35]. However, the surface roughness is not the single factor to determine the surface wettability. Based on previous work [23-27], although the fresh laser treated surfaces showed hierarchical structures, they exhibited super-hydrophilic property with WCA of almost 0º. It is well accepted that surface chemistry is another cause to achieve super-hydrophobic state. Therefore, the difference of surface chemical compositions between the pristine Al-I surface and super-hydrophobic Al-80 surface were examined and discussed in the following section.

3.3 Surface chemical compositions

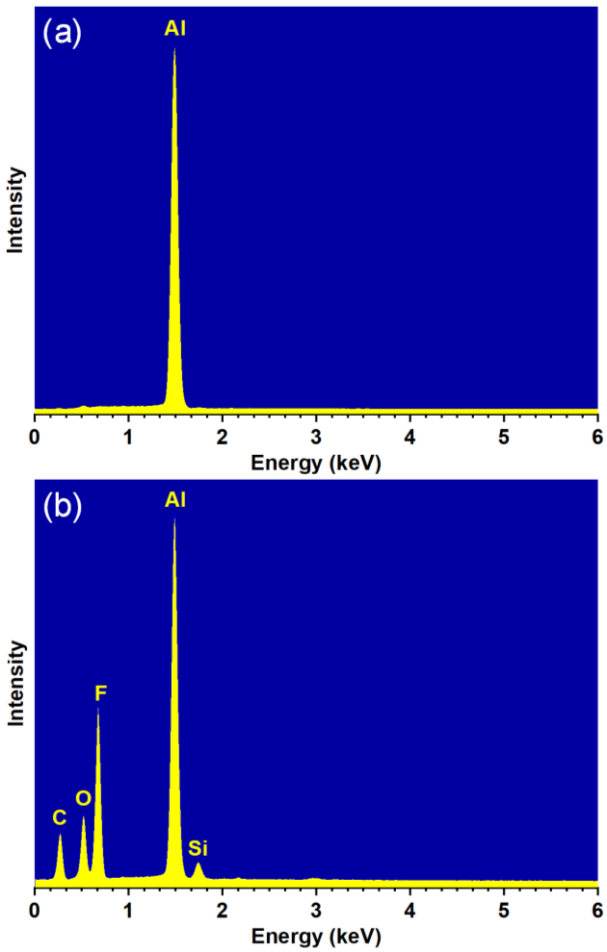

Fig. 6 EDS spectra of (a) pristine Al-I surface and (b) Al-80 super-hydrophobic surface.

EDS spectra of the pristine and super-hydrophobic aluminum surface are shown in Fig. 6. Compared with the pristine surface, it is noted that four additional C, O, F and Si peaks appear on the super-hydrophobic surface after laser treatment and further chemical modification, indicating that the AC-FAS chains have been successfully assembled on the laser treated surface.

In order to further explore the surface chemical compositions of the fabricated super-hydrophobic surface, XPS spectra was elaborately performed. It can be observed from Fig. 7a that the super-hydrophobic surface shows strong signals of C 1s, O 1s, F 1s and a relatively weak signal of Si 2p, which also further revealed that the AC-FAS chains were attached on the laser ablated surfaces. The high-resolution spectra of C 1s is shown in Fig. 7b. It can be deduced that the C 1s peaks centered at 291.8 eV and 294.1 eV belong to the functional groups of $-CF_2-CF_2$ and $-CF_2-CF_3$, respectively [36]. The

peak locating at 289.1 eV was attributed to the functional group of -CH_2-CF_2-. In addition, the peak around 282.0 eV was assigned to carbon atom of C-Si [37]. The carbon atoms of C-C(H) was also detected, locating at the peak of 285.2 eV [38]. Therefore, C 1s spectra can confirm that the super-hydrophobic film contained the functional groups of -CF_2, -CF_3, C-C(H) and C-Si, which derived from the self-absorbed AC-FAS molecules on the laser ablated surface.

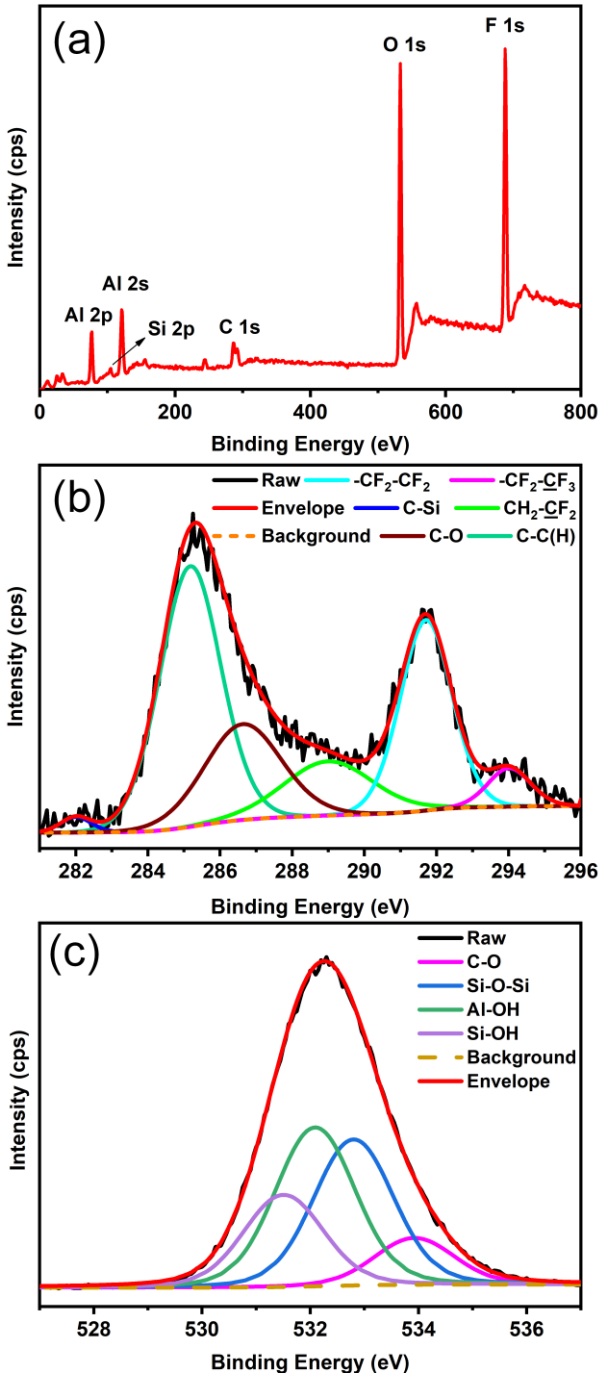

Fig. 7 XPS spectra of Al-80 surface: (a) survey spectra, high-resolution spectra of (b) C 1s and (c) O 1s.

The decomposition of O 1s was also carried out to further analyze the state of oxygen on the super-hydrophobic Al-80 surface. From Fig. 7c, the O 1s peak was fitted with four contributions centered at binding energy around 531.5, 532.3, 532.8 and 533.8 eV, corresponding to Si-OH, Al-OH, Si-O-Si and C-O, respectively [24, 39]. It is obvious that the groups of Si-OH and C-O may come from the AC-FAS molecules, and Al-OH from the laser ablated aluminum surface. However, the existence of Si-O-Si group implies that the cross-linked structures were formed between two AC-FAS molecules during the surface chemical modification process. Based on the analyses of chemical compositions of the as-prepared surface, the formation mechanism of super-hydrophobicity will be extensively explored in the following section.

3.4 Formation mechanism of super-hydrophobicity

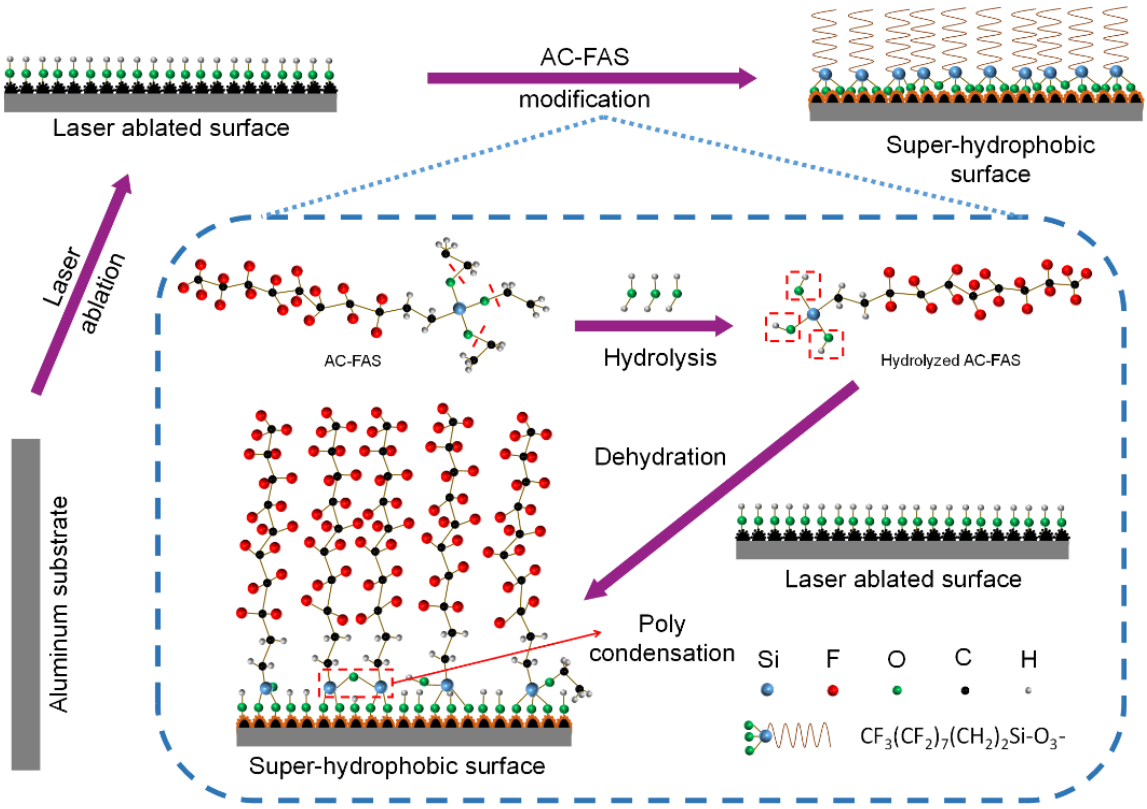

Fig. 8 Formation mechanism of the super-hydrophobic surface with AC-FAS coating on the laser ablated surface.

The hybrid procedure for rapid fabrication of the super-hydrophobic aluminum surfaces is exhibited

in Fig. 8. Immediately after laser ablation, the aluminum substrate presented rough surface with hierarchical structures. However, the initial laser ablated surface presented super-hydrophilic nature rather than super-hydrophobic. This is because more pure aluminum atoms were oxidized due to the localized high temperature, and then quickly transferred to hydrophilic alumina (Al_2O_3) because of the rapid passivation. The alumina surface quickly hydroxylated when it reacted with interfacial water vapor molecules, producing large amount of Al-OH group on the laser ablated surface [40].

When the laser-induced surface was immersed into AC-FAS/ethanol solution, according to the results of surface chemistry, the formation of super-hydrophobic film consisted of three main steps: hydrolysis, dehydration and poly condensation reaction. In the first step, AC-FAS molecule reacted with water, producing the hydrolyzed AC-FAS and ethanol as by-product. Then the obtained hydrolyzed AC-FAS reacted with hydroxyls (Al-OH) under dehydration reaction, resulting in the attachment of long chains of AC-FAS molecules on the laser treated surface. The surface-free-energy can be considerably reduced by the assembled AC-FAS chains. This is because the long chains of AC-FAS molecules had high content of C-F and surface free energies of $-CF_2$ and $-CF_3$ group were only 18 mJ/m^2 and 6.7 mJ/m^2, respectively. Meanwhile, two hydrolyzed AC-FAS molecules could generate cross-linked Si-O-Si functional group under poly condensation reaction, which can further reduce surface free energy and improve surface stability of the attached organic chains. Moreover, it is interesting to find that there was C-O component in both high-resolution of C 1s and O 1s spectra, indicating that the AC-FAS molecules were not fully hydrolyzed. The reminding $O-CH_2-CH_3$ contained nonpolar functional group C-C(H), which also facilitated the laser ablated surface to be super-hydrophobic.

It is noted from Figs. 2-8 that the super-hydrophobic property of fabricated surfaces was determined by the combination of surface morphology and surface chemistry. The laser ablated rough surface with binary structures has been reported to facilitate the surface exhibiting super-hydrophobicity [41-42].

However, it is not sufficient to obtain super-hydrophobicity for the fresh laser ablated surfaces. The further surface chemical modification can rapidly generate super-hydrophobic film in a relatively short time due to the assembled low surface free energy of AC-FAS chains as well as the cross-linked structures. The hierarchical structures combined with the low-free-energy film resulted in a solid-air composite interface as a liquid droplet was placed, and in this case, the surface can be modelled by Cassie-Baxter state. Compared with Al-II surface, the laser ablated hierarchical surface texture had an amplification effect on surface hydrophobicity. It is therefore concluded that generation mechanism of the laser-induced super-hydrophobic surface was attributed to the surface roughness with binary micro/nano surface texture and the presence of low-free-energy fluorinated components onto the as-prepared surfaces.

3.5 Chemical stability and corrosion resistance

Aluminum belongs to active metal and can easily react with acid and base. Therefore, aluminum material has poor chemical stability and corrosion resistance to various corrosive solutions, which limits the practical application of aluminum material. But the as-prepared super-hydrophobic surfaces can significantly reduce the contact area with the corrosive solution and thus prevent the pristine aluminum from reacting with these liquids. To investigate the chemical stability, an 8 μL droplet with different pH values in this study was utilized to measure the static WCA and RA. The hydrochloric acid and sodium hydroxide were used to adjust the pH value of the water droplet. Fig. 9 shows the variations of WCAs and RAs of the super-hydrophobic surface as function of pH value of the droplet. When the pH=1.0, the WCA and RA of the surface were 151.7 ± 1.0º and 8.5 ± 1.0º, indicating that the surface showed good super-hydrophobicity to strong acid solution. With the increase of pH value from 2.0 to 7.0, the static WCA experienced a stable increase and reached a maximum of 160.6 ± 1.5º, while the RA displayed a steady decrease from 8.0 ± 1.0º to 3.0 ± 1.0º. When the pH value of the droplet continuously increased from 7.0 to 13.0, although the WCA slightly decreased and RA increased, the as-prepared surface kept

super-hydrophobic property due to their WCAs more than 150º and RAs less than 10º, indicating that the super-hydrophobic surface can maintain excellent chemical stability in alkaline solutions. Accordingly, the above results sufficiently verified that the acidic and alkaline solutions can hardly make a difference on the wetting property of the fabricated super-hydrophobic surface. Thus, the fabricated super-hydrophobic surfaces had outstanding chemical stability in acidic as well as alkaline environments.

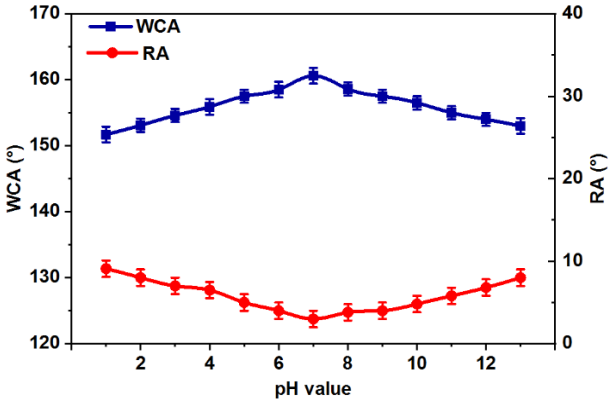

Fig. 9 The variations of WCAs and RAs of the fabricated super-hydrophobic Al-80 surface with different pH value.

In order to study the corrosion resistance of the pristine and super-hydrophobic aluminum surfaces, the potentiodynamic polarization tests were measured in the 3.5 wt. % aqueous NaCl solution as shown in Fig. 10a and the corresponding curves are shown in Fig. 10b. Tafel extrapolation method was used to calculate the corrosion current density (I_{corr}), corrosion potential (E_{corr}) and corrosion rate (CR), as presented in Table 2. In general, a positive-going corrosion potential combined with a low corrosion current density is regarded to behave excellent anti-corrosion property. Therefore, the results demonstrate that the fabricated super-hydrophobic aluminum surface exhibited better anti-corrosion performance than the pristine surface because of its higher corrosion potential (E_{corr}) and smaller corrosion current density (I_{corr}). Compared to pristine aluminum surface, the super-hydrophobic surface possessed a relatively low corrosion rate (CR). Obviously, that the fabricated super-hydrophobic aluminum surface presented better anti-corrosive property than the pristine aluminum substrates.

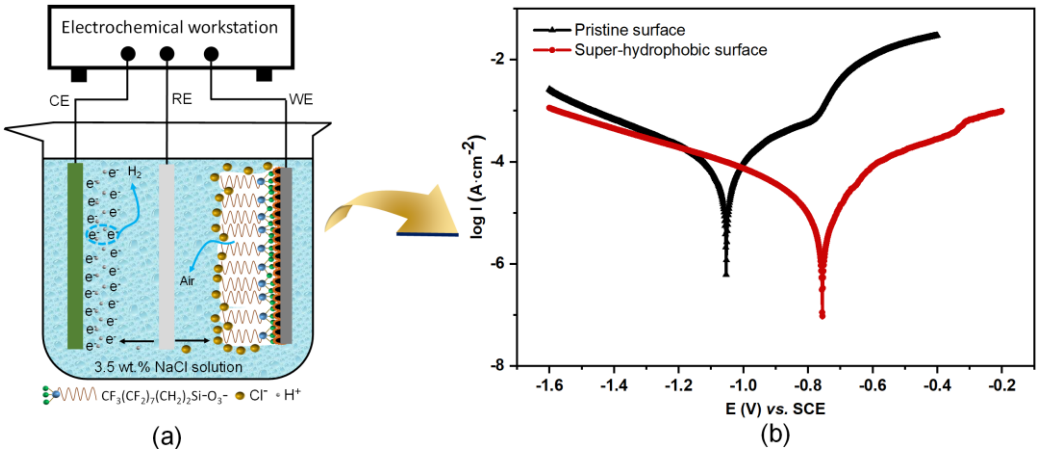

Fig. 10 (a) Schematic diagram of electrochemical measurement: working electrode (WE), counter electrode (CE) and reference electrode (RE), (b) Potentiodynamic polarization curves examined in 3.5 wt. % NaCl solution for pristine Al-I and super-hydrophobic Al-80 surfaces.

Table 2 Corrosion potential (E_{corr}), corrosion current density (I_{corr}) and corrosion rate (CR) of the pristine Al-I and Al-80 surfaces

Sample	E_{corr} (V)	I_{corr} (A cm^{-2})	CR (mm a^{-1})
Pristine surface	-1.06	6.65×10^{-5}	7.26×10^{-1}
Super-hydrophobic surface	-0.75	5.58×10^{-6}	6.08×10^{-2}

The main reason for the chemical stability and corrosion resistance is that the joint effects of hierarchical micro/nano structures and low-free-energy of AC-FAS chains could greatly reduce the contact area between the fabricated super-hydrophobic surface and the corrosive medium. This is because the hierarchical surface texture can create many protrusions, in which air could be trapped based on Cassie-Baxter theory. The huge trapped air could prevent the corrosive ions (Cl^-) from contacting with the super-hydrophobic surface and thus the droplet might be suspended on the surfaces, which will dramatically avoid the chemical reaction between the corrosive water and the fabricated surface. Based on the above explanation, the as-prepared super-hydrophobic surface makes it possible for aluminum material to be applied in severe environments, which will potentially extend the application of aluminum material in engineering.

3.6 Self-cleaning capability and long-term stability

Self-cleaning capability is important for super-hydrophobic surfaces to be applied in engineering [43].

In this work, the self-cleaning capability of the fabricated super-hydrophobic surface was examined by employing a layer of fine chalk dust as contaminant that was uniformly placed on the inclined surface. Fig. 11a shows the mechanism of self-cleaning effect [44]. Compared to the general surface, the water droplet shows a quasi-spherical shape on the super-hydrophobic surfaces. Due to the very small RA, it is very easy for liquid droplets to roll off from the surface and pick up the foreign dust particles at the same time, implying that the dust contaminations show relatively weak adhesion to the super-hydrophobic surface in comparison to the water droplets. Furthermore, the dust contaminants only contact the peak of the micro/nanoscaled structures (shown in Fig. 11a), suggesting that the van der Waals force between the dust and the super-hydrophobic surface is much smaller than the general surface as the contact model is point contact, not a surface contact [45]. Fig. 11b exhibits the evolution process of self-cleaning effect on the laser ablated super-hydrophobic surface. When the water droplets dripped off the syringe needle and trundled on the sample surface, they could completely wipe off the chalk dusts along their rolling paths. This experiment demonstrates that the fabricated super-hydrophobic surface showed a similar self-cleaning effect of lotus leaf. Noticed from **Video 4**, there was no dust particle remaining on the water droplet rolling paths. Finally, after water droplets were free of the surface, the dusted surface became clean, suggesting that the fabricated super-hydrophobic surface possessed excellent self-cleaning capability. Therefore, it is concluded that the laser-induced super-hydrophobic surface can protect the aluminum material from pollution in practical applications.

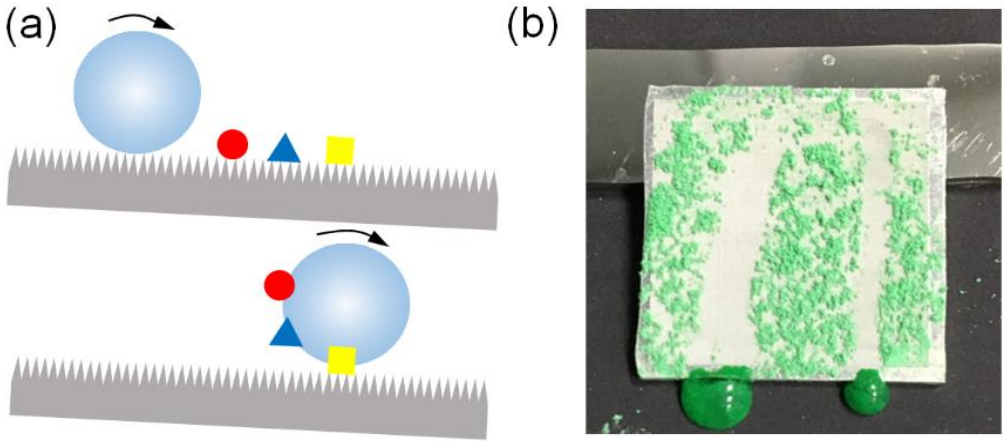

Fig. 11 (a) Schematic depicting the motion of water droplet covered with dust on inclined super-hydrophobic surface, (b) Self-cleaning effect of super-hydrophobic surface (Al-80).

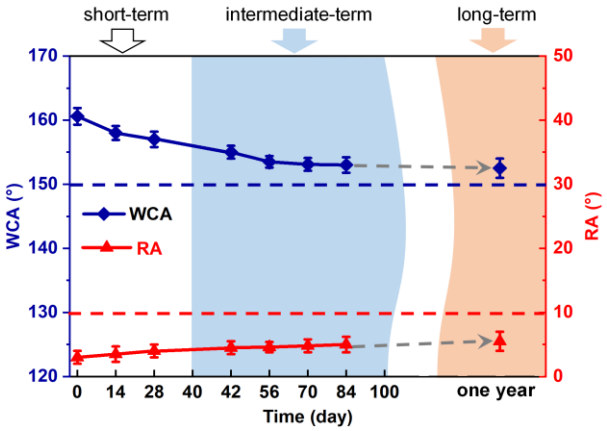

Fig. 12 Time dependence of WCAs and RAs of Al-80 surface under ambient air.

Furthermore, the stability of the super-hydrophobic surfaces in ambient air was also investigated in this study. Fig. 12 demonstrates that the as-prepared surface could maintain outstanding super-hydrophobicity for short- (40 days) and intermediate-term (100 days) although the WCA showed a slight decrease and the RA showed a negligible increase [46]. After three months stored in the ambient air, the as-prepared surface exhibited a WCA of 153.1 ± 1.5º with the RA of 5.0 ± 1.5º. Even one year later, the fabricated super-hydrophobic surface also presented super-hydrophobic property with the WCA of 152.2 ± 1.5º and the RA of 6.0 ± 1.5º. Thus, the produced super-hydrophobic film was very stable and it could maintain long-term stability in ambient air due to its WCA greater than 150º and RA less than 10º.

4 Conclusion

In this work, the super-hydrophobic aluminum surfaces have been rapidly fabricated via the hybrid nanosecond laser ablation process and silanization modification of AC-FAS. The whole processing time can be controlled within a striking several hours instead of 30 days under ambient air exposure. The surface morphology and roughness can be slightly adjusted by pitch effect, but resulting in similar super-hydrophobicity. The WCA of the as-prepared surfaces can reach up to 160.6 ± 1.5º with small RA of 3.0 ± 1.0º. Based on the SEM/3D images and EDS/XPS spectra, the formation mechanism of super-hydrophobicity can be ascribed to the hierarchical structures (containing both microscale protrusions/pillars and nanoscale particles) due to nanosecond laser ablation and the presence of low-free-energy fluorinated chains because of the post chemical modification. In addition, the elaborate experiments were conducted to prove the fabricated super-hydrophobic surface exhibiting outstanding super-hydrophobicity in various pH values, better anti-corrosion performance in 3.5 wt. % NaCl solution, excellent self-cleaning effect and long-term stability in the ambient air. More importantly, the reasons for above examined properties of the super-hydrophobic surface were also proposed to make a better understanding of super-hydrophobic surface, which will raise the promising prospects of aluminum material for application. This time-saving, low-cost and facile laser ablation and post chemical modification definitely offers an effectively and promising technique for quantity production of super-hydrophobic aluminum surfaces, which can extend the applications of aluminum material in engineering.

Acknowledgments

This work received funding supports from H2020 Project (FabSurfWAR-644971), National Key R&D Program of China (No. 2017YFB1104700), Program of International S&T Cooperation (2016YFE0112100) and National Natural Science Foundations of China (Nos. 51675371, 51675376 and 51675367). The authors gratefully acknowledge Professor Zuobin Wang in Changchun University

of Science and Technology for the technical supports. Z. Yang also acknowledges the financial support from China Scholarship Council (CSC).

References

[1] Huhtamäki T, Tian X L, Korhonen J T, Ras R H A. Surface-wetting characterization using contact-angle measurements. *Nature Protocols*, 2018, **13**, 1521-1538.

[2] Barthlott W, Neinhuis C. Purity of the sacred lotus, or escape from contamination in biological surfaces. *Planta*, 1997, **202**, 1-8.

[3] Parker A. R, Lawrence C R. Water capture by a desert beetle. *Nature*, 2001, **414**, 33-34.

[4] Gao X F, Jiang L. Water-repellent legs of water striders. *Nature*, 2004, **432**, 36.

[5] Gao X Y, Guo Z G. Biomimetic superhydrophobic surfaces with transition metals and their oxides: A review. *Journal of Bionic Engineering*, 2017, **14**, 401-439.

[6] Qi X, Song W, Mao Z, Gao W R, Cong Q. Fabrication of a Bionic Needle with both Super-Hydrophobic and Antibacterial Properties. *Journal of Bionic Engineering*, 2013, **10**, 377-382.

[7] Song Y, Liu Y, Zhan B, Kaya C, Stegmaier T, Han Z W, Ren L Q. Fabrication of bioinspired structured superhydrophobic and superoleophilic copper mesh for efficient oil-water separation. *Journal of Bionic Engineering*, 2017, **14**, 497-505.

[8] Trdan U, Hočevar M, Gregorčič P. Transition from superhydrophilic to superhydrophobic state of laser textured stainless steel surface and its effect on corrosion resistance. *Corrosion Science*, 2017, **123**, 21-26.

[9] Doll K, Fadeeva E, Stumpp N S, Grade S, Chichkov B N, Stiesch M. Reduced bacterial adhesion on titanium surfaces micro-structured by ultra-short pulsed laser ablation. *BioNanoMaterials*, 2016, **17**, 53-57.

[10] Hsieh C T, Chen J M, Kuo R R, Lin T S, Wu C F. Influence of surface roughness on water- and

oil-repellent surfaces coated with nanoparticles. *Applied Surface Science*, 2005, **240**, 318-326.

[11] Yong J L, Chen F, Yang Q, Bian H, Du G Q, Shan C, Huo J L, Fang Y, Hou X. Oil-water separation: a gift from the desert. *Advanced Materials Interfaces*, 2016, **3**, 1500650.

[12] Bhushan B, Jung Y C. Natural and biomimetic artificial surfaces for superhydrophobicity, self-cleaning, low adhesion, and drag reduction. *Progress Materials Science*, 2011, **56**, 1-108.

[13] Feng L, Li S H, Li Y S, Li H J, Zhang L J, Zhai J, Song Y L, Liu B Q, Jiang L, Zhu D B. Super-hydrophobic surfaces: from natural to artificial. *Advanced Materials*, 2002, **14**, 1857-1860.

[14] Ellinas K, Tserepi A, Gogolides E. From superamphiphobic to amphiphilic polymeric surfaces with ordered hierarchical roughness fabricated with colloidal lithography and plasma nanotexturing. *Langmuir*, 2011, **27**, 3960-3969.

[15] Toosi S F, Moradi S, Ebrahimi M, Hatzikiriakos S G. Microfabrication of polymeric surfaces with extreme wettability using hot embossing. *Applied Surface Science*, 2016, **378**, 426-434.

[16] Steele A, Bayer I, Moran S, Cannon A, King W P, Loth E. Conformal ZnO nanocomposite coatings on micro-patterned surfaces for superhydrophobicity. *Thin Solid Films*, 2010, **518**, 5426-5431.

[17] Hwang S J, Oh D J, Jung P G, Lee S M, Go J S, Kim J H. Dry etching of polydimethylsiloxane using microwave plasma. *Journal of Micromechanics and Microengineering*, 2009, **19**, 1489-1503.

[18] Goto Y, Takashima H, Takishita K, Sawada H. Creation of coating surfaces possessing superhydrophobic and superoleophobic characteristics with fluoroalkyl end-capped vinyltrimethoxysilane oligomeric nanocomposites having biphenylene segments. *Journal of Colloid Interface Science*, 2011, **362**, 375-381.

[19] Yang Z, Liu X P, Tian Y L. Fabrication of super-hydrophobic nickel film on copper substrate with improved corrosion inhibition by electrodeposition process. *Colloids and Surface A*, 2019, **560**,

205-212.

[20] Cardoso J T, Garcia-Girón A, Romano J M, Huerta-Murillo D, Jagdheesh R, Walker M, Dimov S S, Ocaña J L. Influence of ambient conditions on the evolution of wettability properties of an IR-, ns-laser textured aluminium alloy, *RSC Adv*, 2017, **7**, 39617-39627.

[21] Chun D M, Ngo C V, Lee K M. Fast fabrication of superhydrophobic metallic surface using nanosecond laser texturing and low-temperature annealing. *CIRP Annals-Manufacturing Technology*, 2016, **65**, 519-522.

[22] Ta D V, Dunn A, Wasley T J, Kay R W, Stringer J, Smith P J, Connaughton C, Shephard J D. Nanosecond laser ablated superhydrophobic metallic surfaces and their chemical sensing applications. *Applied Surface Science*, 2015, **357**, 248-254.

[23] Kietzig A M, Hatzikiriakos S G, Englezos P. Patterned superhydrophobic metallic surfaces. *Langmuir*, 2009, **25**, 4821-4827.

[24] Long J, Zhong M, Zhang H, Fan P. Superhydrophilicity to superhydrophobicity transition of picosecond laser microstructured aluminum in ambient air. *Journal of Colloid Interface Science*, 2015, **441**, 1-9.

[25] Jagdheesh R, García-Ballesteros J J, Ocaña J L. One-step fabrication of near superhydrophobic aluminum surface by nanosecond laser ablation. *Applied Surface Science*, 2016, **374**, 2-11.

[26] Yang Z, Tian Y L, Yang C J, Wang F J, Liu X P. Modification of wetting property of Inconel 718 surface by nanosecond laser texturing. *Applied Surface Science*, 2017, **414**, 313-324.

[27] Yang C J, Mei X S, Tian Y L, Zhang D W, Li Y, Liu X P. Modification of wettability property of titanium by laser texturing. *The International Journal of Advanced Manufacturing Technology*, 2016, **87**, 1663-1670.

[28] Tian Y L, Zhao Y C, Yang C J, Wang F J, Liu X P, Jing X B. Fabrication of bio-inspired nitinol alloy surface with tunable anisotropic wetting and high adhesive ability. *Journal of Colloid*

Interface Science, 2018, **527**, 328-338.

[29] Long J, Zhong M, Fan P, Gong D, Zhang H. Wettability conversion of ultrafast laser structured copper surface. *Journal of Laser Applications*, 2015, **27**, S29107.

[30] Boinovich L B, Emelyanenko A M, Emelyanenko K A, Domantovsky A G, Shiryaev A A. Comment on "Nanosecond lase textured superhydrophobic metallic surfaces and their chemical sensing applications" by Duong V. Ta, Andrew Dunn, Thomas J. Wasley, Robert W. Kay, Jonathan Stringer, Patrick J. Smith, Colm Connaughton, Jonathan D. Shephard (Appl. Surf. Sci. 357 (2015) 248-254). *Applied Surface Science*, 2016, **379**, 111-113.

[31] Davaasuren G, Ngo C V, Oh H S, Chun D M. Geometric study of transparent superhydrophobic surfaces of molded and grid patterned polydimethylsiloxane (PDMS). *Applied Surface Science*, 2014, **314**, 530-536.

[32] Tang M K, Huang X J, Guo Z, Yu J G, Li X W, Zhang Q X. Fabrication of robust and stable superhydrophobic surface by a convenient, low-cost and efficient laser marking approach. *Colloids and Surface A*, 2015, **484**, 449-456.

[33] Chen Z, Hao L M, Chen A Q, Song Q J, Chen C L. A rapid one-step process for fabrication of superhydrophobic surface by electrodeposition method. *Electrochimica Acta*, 2012, **59**, 168-171.

[34] Tan J Y, Hao J J, An Z Q, Liu Z S. Simple fabrication of superhydrophobic nickel surface on steel substrate via electrodeposition. *International Journal of Electrochemical Science*, 2017, **12**, 40-49.

[35] Erbil H Y, Cansoy C E. Range of applicability of the Wenzel and Cassie-Baxter equations for superhydrophobic surfaces. *Langmuir*, 2009, **25**, 14135-14145.

[36] Hozumi A, Ushiyama K, Sugimura H, Takai O. Fluoroalkylsilane monolayers formed by chemical vapor surface modification on hydroxylated oxide surfaces. *Langmuir*, 1999, **15**, 7600-7604.

[37] Saleema N, Sarkar D K, Paynter R W, Chen X G. Superhydrophobic aluminum alloy surfaces by a

novel one-step process. *ACS Applied Materials & Interfaces*, 2010, **2**, 2500-2502.

[38] Su F H, Yao K. Facile Fabrication of superhydrophobic surface with excellent mechanical abrasion and corrosion resistance on copper substrate by a novel method. *ACS Applied Materials & Interfaces*, 2014, **6**, 8762-8770.

[39] Birdianu I E, David G, Simionescu B, Aflori M, Ursu C, Coroaba A, Hitruc G, Cotofana C, Olaru M. Functional silsesquioxane-based hierarchical assemblies for antibacterial/antifungal coatings. *Journal of Materials Chemistry B*, 2015, **3**, 723-727.

[40] Yang Z, Tian Y L, Liu X P. Insights into the wettability transition of nanosecond laser ablated surface under ambient air exposure. *Journal of Colloid & Interface Science*, 2019, **533**, 268-277.

[41] Liu K, Zhang M, Zhai J, Wang J, Jiang L. Bioinspired construction of Mg-Li alloys surfaces with stable superhydrophobicity and improved corrosion resistance. *Applied Physics Letters*, 2008, **92**, 183103.

[42] Xu W J, Song J L, Sun J, Lu Y, Yu Z Y. Rapid fabrication of large-area, corrosion-resistant superhydrophobic Mg alloy surfaces. *ACS Applied Materials & Interfaces*, 2011, **3**, 4404-4414.

[43] Liu Y, Liu J D, Li S Y, Han Z W, Yu S R, Ren L Q. Fabrication of biomimetic super-hydrophobic surface on aluminum alloy. *Journal of Materials Science*, 2014, **49**, 1624-1629.

[44] Liu Xue C H, Jia S T, Zhang J, Ma J Z. Large-area fabrication of superhydrophobic surfaces for practical applications: an overview. *Science and Technology of Advanced Materials*, 2010, **11**, 033002.

[45] Yong J L, Yang Q, Chen F, Zhang D S, Farooq U, Du G Q, Hou X. A simple way to achieve superhydrophobicity, controllable water adhesion, anisotropic sliding, and anisotropic wetting based on femtosecond laser-induced line-patterned surfaces. *Journal of Materials Chemistry A*, 2014, **2**, 5499-5507.

[46] Gregorčič P, Conradi, M, Hribar, L, Hočevar M. Long-term influence of laser-processing

parameters on (super)hydrophobicity development and stability of stainless-steel surfaces. *Materials*, 2018, **11**, 2240.